



HAL
open science

Fast cracks in high-speed photographs of shocked diamond

Geoffrey Willmott, John Field

► **To cite this version:**

Geoffrey Willmott, John Field. Fast cracks in high-speed photographs of shocked diamond. *Philosophical Magazine*, 2006, 86 (27), pp.4305-4318. 10.1080/14786430500482336 . hal-00513642

HAL Id: hal-00513642

<https://hal.science/hal-00513642>

Submitted on 1 Sep 2010

HAL is a multi-disciplinary open access archive for the deposit and dissemination of scientific research documents, whether they are published or not. The documents may come from teaching and research institutions in France or abroad, or from public or private research centers.

L'archive ouverte pluridisciplinaire **HAL**, est destinée au dépôt et à la diffusion de documents scientifiques de niveau recherche, publiés ou non, émanant des établissements d'enseignement et de recherche français ou étrangers, des laboratoires publics ou privés.

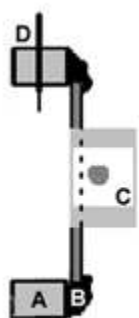
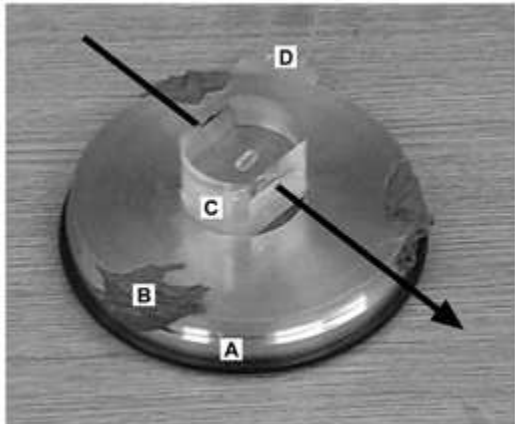


Fast cracks in high-speed photographs of shocked diamond

Journal:	<i>Philosophical Magazine & Philosophical Magazine Letters</i>
Manuscript ID:	TPHM-05-Mar-0066.R2
Journal Selection:	Philosophical Magazine
Date Submitted by the Author:	29-Sep-2005
Complete List of Authors:	Willmott, Geoffrey; University of Cambridge, Physics Field, John; University of Cambridge, Physics
Keywords:	high-speed photography, diamond, cracks
Keywords (user supplied):	
<p>Note: The following files were submitted by the author for peer review, but cannot be converted to PDF. You must view these files (e.g. movies) online.</p>	
CracksPaper.tex	



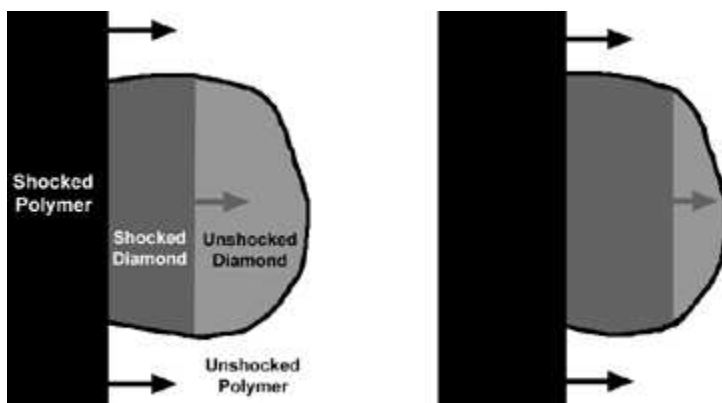
1
2
3
4
5
6
7
8
9
10
11
12
13
14
15
16
17
18
19
20
21
22
23
24
25
26
27
28
29
30
31
32
33
34
35
36
37
38
39
40
41
42
43
44
45
46
47
48
49
50
51
52
53
54
55
56
57
58
59
60



130x77mm (72 x 72 DPI)

er Review Only

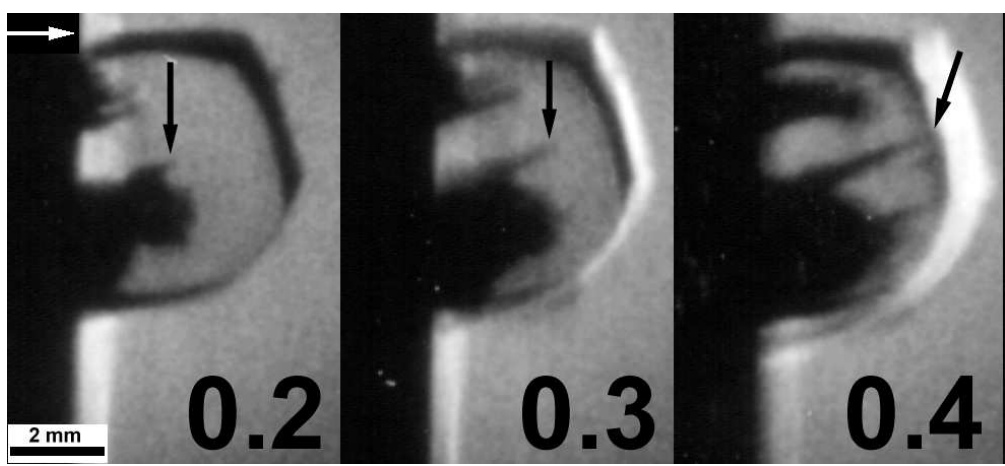
1
2
3
4
5
6
7
8
9
10
11
12
13
14
15
16
17
18
19
20
21
22
23
24
25
26
27
28
29
30
31
32
33
34
35
36
37
38
39
40
41
42
43
44
45
46
47
48
49
50
51
52
53
54
55
56
57
58
59
60



130x69mm (72 x 72 DPI)

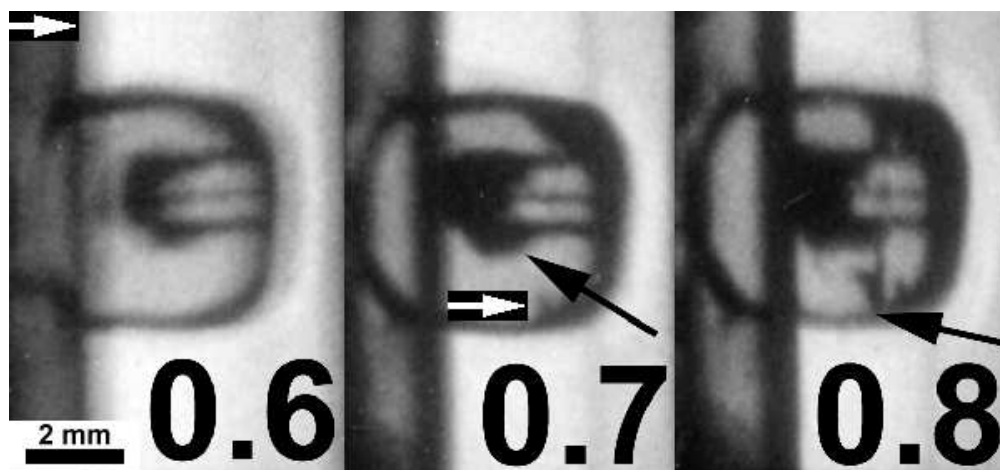
Peer Review Only

1
2
3
4
5
6
7
8
9
10
11
12
13
14
15
16
17
18
19
20
21
22
23
24
25
26
27
28
29
30
31
32
33
34
35
36
37
38
39
40
41
42
43
44
45
46
47
48
49
50
51
52
53
54
55
56
57
58
59
60



347x156mm (72 x 72 DPI)

Review Only

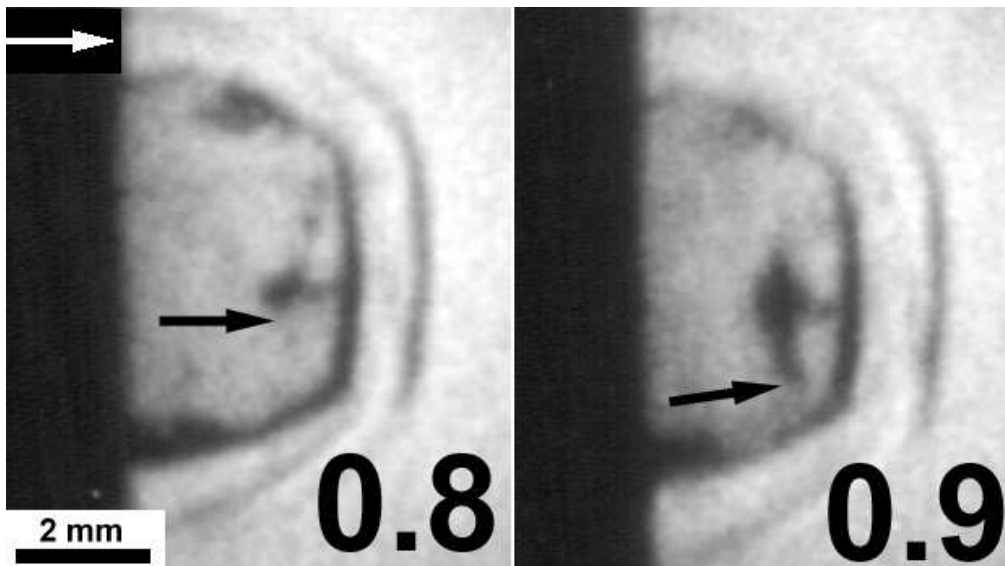


211x98mm (72 x 72 DPI)

Review Only

1
2
3
4
5
6
7
8
9
10
11
12
13
14
15
16
17
18
19
20
21
22
23
24
25
26
27
28
29
30
31
32
33
34
35
36
37
38
39
40
41
42
43
44
45
46
47
48
49
50
51
52
53
54
55
56
57
58
59
60

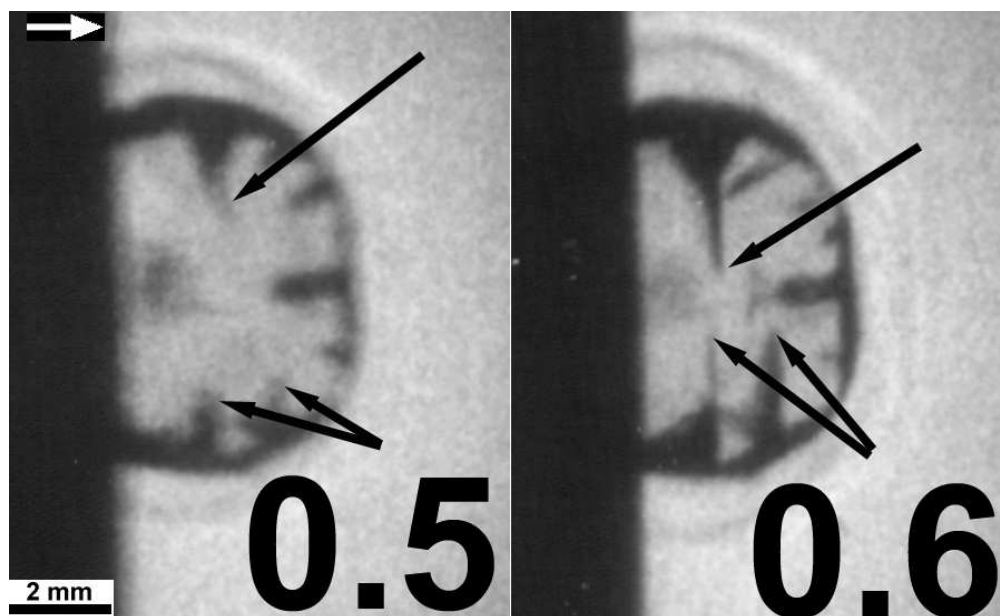
1
2
3
4
5
6
7
8
9
10
11
12
13
14
15
16
17
18
19
20
21
22
23
24
25
26
27
28
29
30
31
32
33
34
35
36
37
38
39
40
41
42
43
44
45
46
47
48
49
50
51
52
53
54
55
56
57
58
59
60



217x122mm (72 x 72 DPI)

Review Only

1
2
3
4
5
6
7
8
9
10
11
12
13
14
15
16
17
18
19
20
21
22
23
24
25
26
27
28
29
30
31
32
33
34
35
36
37
38
39
40
41
42
43
44
45
46
47
48
49
50
51
52
53
54
55
56
57
58
59
60



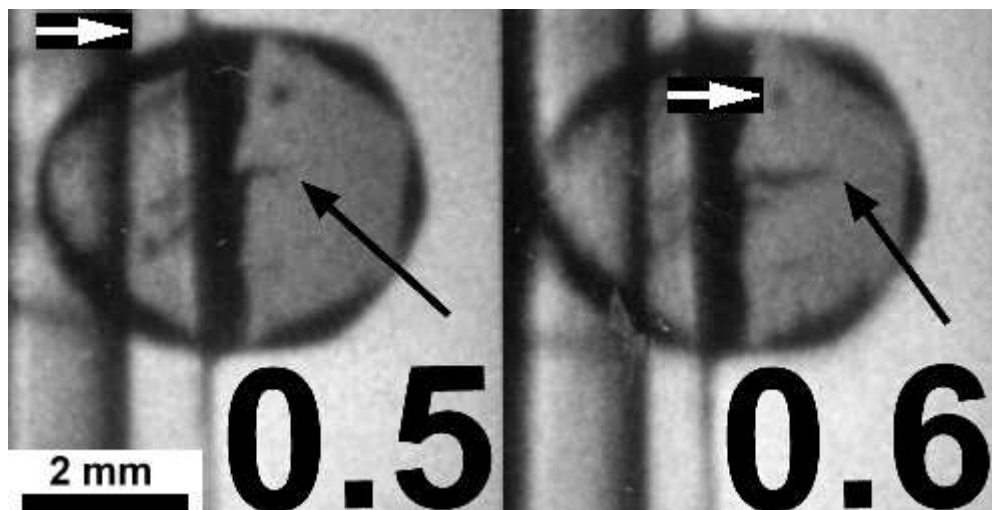
317x194mm (72 x 72 DPI)

Review Only

1
2
3
4
5
6
7
8
9
10
11
12
13
14
15
16
17
18
19
20
21
22
23
24
25
26
27
28
29
30
31
32
33
34
35
36
37
38
39
40
41
42
43
44
45
46
47
48
49
50
51
52
53
54
55
56
57
58
59
60



130x166mm (600 x 600 DPI)

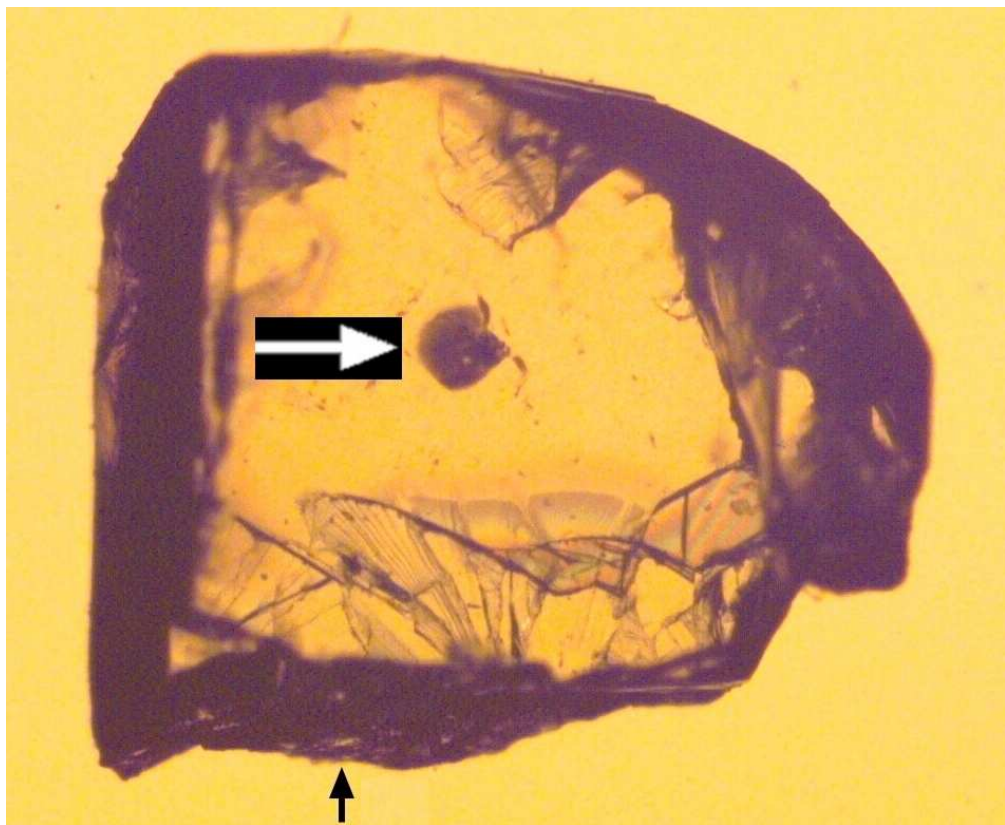


174x89mm (72 x 72 DPI)

Review Only

1
2
3
4
5
6
7
8
9
10
11
12
13
14
15
16
17
18
19
20
21
22
23
24
25
26
27
28
29
30
31
32
33
34
35
36
37
38
39
40
41
42
43
44
45
46
47
48
49
50
51
52
53
54
55
56
57
58
59
60

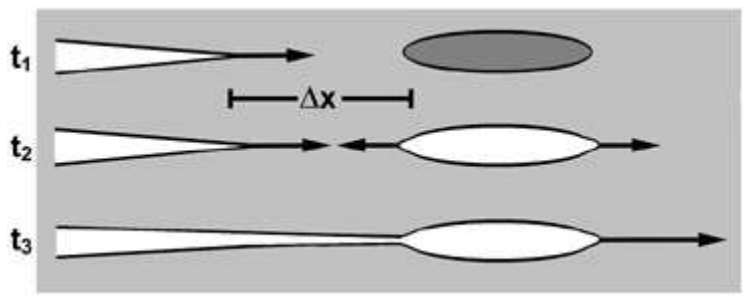
1
2
3
4
5
6
7
8
9
10
11
12
13
14
15
16
17
18
19
20
21
22
23
24
25
26
27
28
29
30
31
32
33
34
35
36
37
38
39
40
41
42
43
44
45
46
47
48
49
50
51
52
53
54
55
56
57
58
59
60



334x274mm (72 x 72 DPI)

Manuscript Only

1
2
3
4
5
6
7
8
9
10
11
12
13
14
15
16
17
18
19
20
21
22
23
24
25
26
27
28
29
30
31
32
33
34
35
36
37
38
39
40
41
42
43
44
45
46
47
48
49
50
51
52
53
54
55
56
57
58
59
60



130x55mm (72 x 72 DPI)

Peer Review Only

Fast cracks in high-speed photographs of shocked diamond

G. R. Willmott and J. E. Field

Physics and Chemistry of Solids, Cavendish Laboratory,

Madingley Rd, Cambridge CB3 0HE, UK

Phone: (44) (0)1223 339375

Fax: (44) (0)1223 350266

Email: grw23@cam.ac.uk

Six fracture surfaces have been observed extending at velocities between c_R (the Rayleigh wave velocity) and $1.3c_R$ in high-speed photographs of four diamond specimens. The diamonds were embedded in a transparent polymer and shocked in plate impact experiments. The measured velocities exceed limiting velocities proposed in theoretical and practical studies of single mode I cracks in diamond. The fracture surfaces probably extend by initiation and coalescence of multiple tensile fractures along a single cleavage plane. This mechanism is dependent on the suppression of cracks branching from the $\{111\}$ growth plane in diamond and considers the population of flaws near a propagating crack tip.

Keywords: Diamond; Cracks; High-speed photography

1 Introduction

Analysis of the onset of brittle fracture began with Griffith's seminal paper, in which the tensile stress required to extend an ideal single crack in an isotropic brittle solid was derived [1]. Griffith's approach, which considered mechanical and free surface energies, has been used to describe brittle fracture in numerous and varied applications [2]. Mott [3] extended Griffith's work to the analysis of propagating cracks by considering kinetic energy. Theoretical analyses of brittle fracture have since focussed on crack propagation in solids that have a linear elastic constitutive response up to failure (perfectly brittle) and are isotropic and homogeneous (monolithic) in terms of constitutive response and fracture toughness. This mathematically complex topic has been dealt with at length in modern summaries by Broberg [4] and Freund [5].

A common feature of analytic solutions for single mode I cracks is that the crack velocity (v) approaches asymptotically the Rayleigh (surface) wave velocity (c_R), which is $\sim 90\%$ of the shear wave velocity (c_S) and significantly less than the longitudinal wave velocity (c_L). It seems physically reasonable that the speed of a crack should be limited by the speed at which waves can propagate along the free surface it creates. This limit has been verified in experiments using various techniques (including high-speed photography) to record crack velocities in a variety of materials [6]. Cracks were observed propagating at up to $0.88c_R$ along a preferred cleavage plane in magnesium oxide. In general, single tensile cracks run at velocities up to a practical limit of $\sim 0.6c_R$, at which point branching occurs.

Experiments in isotropic materials (e.g. [7]) have shown that cracks are most easily initiated and propagate preferentially along pathways for which the stress at the crack tip is purely tensile. In an anisotropic material, pure mode I crack propagation can be energetically unfavourable, in which case a crack can propagate with mixed-mode loading. The problem of mode II cracks moving along predetermined

1
2
3
4
5
6
7
8 weak paths has been a subject of some interest over the past decade due to the
9 development of specialized, inhomogeneous engineering materials and geophysical
10 reports of ‘inter-sonic’ average fault plane rupture velocities [8]. For an inter-sonic
11 crack, $c_S < v < c_L$, Rosakis et al. [9] have observed inter-sonic mode II fractures
12 on a weakened plane in a polymer using high-speed photography and a dynamic
13 photoelasticity technique. The cracks were accompanied by multiple conchoidal
14 fractures in directions perpendicular to the crack path.
15
16
17
18
19
20

21 Rosakis [7] has reviewed the phenomenon of inter-sonic shear rupture along a
22 predetermined weak plane in an otherwise monolithic material. There is a singular
23 analytic solution for the stress field at the tip of a mode II inter-sonic crack [10]. The
24 physical implication of this solution is that shear cracks should be able to propagate
25 at $v = \sqrt{2}c_S$. Analytical and modelling studies which incorporate non-steady-state
26 solutions with finite process zones have described possible mechanisms for shear
27 cracks propagating at speeds greater than c_S other than $\sqrt{2}c_S$. The Burridge-
28 Andrews mechanism has become widely accepted due to corroborating results from
29 other numerical studies [7].
30
31
32
33
34
35
36
37

38 Griffith [1] also noticed that flaw populations have a significant effect on the
39 strength of apparently perfect materials. In tension, flaws will evolve into cracks if
40 they are large or located in regions where the stresses are large. Any macroscopic
41 specimen of a brittle material contains a microscopic population of flaws. The
42 genesis, size and distribution of flaws in brittle solids have been discussed by Lawn
43 [2].
44
45
46
47
48

49 The current paper reports experimental measurements of fracture velocities
50 from well-calibrated high-speed photographic sequences of shocked diamond. The
51 implications of these measurements, in which some cracks appear to move faster
52 than c_R , are interpreted in the context of previous work. Due consideration is given
53 to the role of flaws that lie near a propagating crack tip in a real material. A mech-
54
55
56
57
58
59
60

1
2
3
4
5
6
7
8 anism for extension of fracture surfaces in tension at velocities greater than c_R is
9 described.
10

11 Diamond has an extremely stable covalent lattice that is responsible for many
12 extreme physical characteristics, making it suitable for a wide range of industrial
13 and technological applications. It is often considered ‘perfectly brittle’, so it is
14 the ideal material to compare with analytical approaches to fracture mechanics.
15 The anisotropy of diamond, in which the $\{111\}$ crystallographic plane dominates
16 cleavage, suppresses crack branching and encourages propagation of high velocity
17 cracks. Field [6] has previously measured a crack velocity of $7.2 \text{ mm } \mu\text{s}^{-1}$ ($0.7c_R$)
18 in high-speed photographs of diamond. A limited number of specimens were used
19 and Field noted that the maximum velocity for cracks in diamond could be higher.
20
21
22
23
24
25
26
27
28
29

30 **2 Experimental**

31 **2.1 Diamond**

32 [Insert table 1 about here]

33 Diamond is a form of pure elemental carbon in which each atom has four tetra-
34 hedral sp^3 bonds with its nearest neighbours. The diamond lattice has a high
35 coordination number (4), strong bonds, short bond length (0.154 nm) and a stable
36 structure. Pure diamond is transparent in optical light. Other physical properties
37 are summarized in table 1. Field and Freeman’s [11] experimental value of γ_{111}
38 from indentation is $5.50 \pm 0.15 \text{ J m}^{-2}$, and close enough to theory to suggest that
39 plastic deformation at the crack tip is negligible. A summary of research into the
40 strength, fracture and erosion properties of diamond has been compiled by Field
41 [12].
42
43
44
45
46
47
48
49
50
51
52
53

54 Most natural diamonds grow by deposition of successive layers on $\{111\}$ facets,
55 so that the shape of recovered diamonds is that of interlinking $\{111\}$ planes: an
56
57
58
59
60

1
2
3
4
5
6
7
8 octahedron. The {111} crystallographic plane is the dominant cleavage plane in
9 diamond, as first noted by Ramaseshan [13]. A static crack on a {111} plane will
10 not extend on a different crystallographic plane, regardless of the loading conditions
11 applied [14]. A first-principles quantum mechanical approach [15] has shown that
12 the tensile strength of a perfect diamond crystal is lowest in the $\langle 111 \rangle$ direction.
13 Flaws and inclusions that encourage cleavage are likely to lie on growth planes; the
14 tensile strength derived from indentation experiments (table 1) is a factor of 50 less
15 than theoretical calculations.
16

17
18 By taking into account the crystallographic variation of elastic moduli in di-
19 amond and possible confinement states, extreme values of c_L and c_S in diamond
20 have been calculated. The range of possible values is 17.3–19.5 mm μs^{-1} for c_L
21 and 10.5–13.0 mm μs^{-1} for c_S . Viktorov [16], who has given a full description of
22 Rayleigh waves, suggests the following approximate formula for calculation of c_R :
23

$$c_R = \left(\frac{0.87 + 1.12\nu}{1 + \nu} \right) c_S \quad (1)$$

24
25 Considering the full range of possible values for c_S and ν , c_R can take a range
26 of values between 9.6 and 11.4 mm μs^{-1} . Applied hydrostatic [17] or shock [18]
27 compression can also alter the elastic properties of a material. Under shock con-
28 ditions similar to those in the current experiments, c_L does not increase by more
29 than 15 % from the ambient value in metallic solids.
30
31

32 33 34 35 36 37 38 39 40 41 42 43 44 45 46 47 **2.2 High-Speed Photography**

48
49 High-speed photography is probably the most data-rich diagnostic technique for
50 shock events involving transparent materials. High-speed cameras capture pho-
51 tographs, or ‘frames’, in time-ordered sequences. The image in each frame is gen-
52 erated using light that enters the camera during the exposure time for that frame.
53 The interframe time (IFT) is the interval between the start of successive exposures.
54
55
56
57
58
59
60

1
2
3
4
5
6
7
8 Modern summaries of the history and applications of high-speed photography have
9 been compiled by Field [19] and Ray [20].

10
11 An image-converter camera, the IMCO Ultramac 501, was used in the current
12 research. This camera can produce between 8 and 24 frames at framing rates up
13 to $2 \times 10^7 \text{ s}^{-1}$, with a minimum exposure time of 10 ns. The IFT and exposure
14 time are fully programmable for each frame. Images are produced as good-quality
15 Polaroid prints.
16
17

18
19 In the current study, black and white photographs of shock waves and fracture
20 in transparent brittle solids are of interest. In a uniformly illuminated transparent
21 material, a shock front is imaged as a dark line due to a shock-induced discontinuity
22 in the refractive index across the wave front ('Schlieren' contrast). A fracture is
23 imaged as a dark line once the crack is wider than half the wavelength of the
24 illuminating light, or 200–350 nm for white light. If a fracture plane is parallel to
25 the angle of view, the crack will appear sharp; thicker fractures lie on oblique angles.
26 Cracks sometimes 'disappear' in high-speed sequences when fracture surfaces are
27 pushed together [21].
28
29
30
31
32
33
34
35
36
37
38

39 **2.3 *Embedded Diamond Experiments***

40
41 An experimental technique was developed in order to view the effects of shock waves
42 on transparent diamond specimens. Nine specially prepared, polished slices of type
43 IaA diamond (diameter ~5 mm and thickness 1–2 mm) were made available for the
44 current study [14]. Specimens were either 'good quality' (containing no macroscopic
45 flaws) or 'cracked' (with visible fracture surfaces). Each diamond was embedded in
46 a matrix of polymethylmethacrylate (PMMA), which was synthesized by heating
47 and pressing a powder. The uniform pressure applied to the powder was 0.02 GPa
48 and the polymer was cooled slowly to avoid trapping internal stresses.
49
50
51
52
53
54
55

56 [Insert figure 1 about here]
57
58
59
60

1
2
3
4
5
6
7
8
9
10
11
12
13
14
15
16
17
18
19
20
21
22
23
24
25
26
27
28
29
30
31
32
33
34
35
36
37
38
39
40
41
42
43
44
45
46
47
48
49
50
51
52
53
54
55
56
57
58
59
60

Planar shock waves were induced in the PMMA blocks using the plate impact technique in the single-stage light gas gun at the Cavendish Laboratory [22]. Target geometry is shown in figure 1. Target and flyer plates were machined flat and parallel to within $\pm 5 \mu\text{m}$. At impact, the plates are aligned to within $\pm 0.5 \text{ mrad}$ using a mechanical alignment dial gauge. Copper flyer plates of thickness 3 mm were mounted on polycarbonate sabots, with a recess behind each flyer plate providing a free rear surface. A series of shorting pins and a specially designed ‘make’ trigger were used to trigger diagnostics precisely and measure impact velocity (accurate to within $\pm 0.5 \%$) for each experiment. Shock waves had a ‘top hat’ profile, with duration determined by the thickness of the flyer plate and the well-known velocity of shock waves in copper.

When the shock wave reached the embedded disc, high-speed photographs were taken. Each embedded particle had polished faces normal to the line-of-sight of the camera. The sides of each polymer plate were flattened and polished parallel to the particle faces so that light entering the camera was not significantly refracted by the transparent solids. Therefore, the diamonds were fixed in a carefully aligned, mounted position, in order to allow the camera and flash to be triggered with high precision.

[Insert figure 2 about here]

Photographic images of the embedded diamonds are obscured by the shock wave in the PMMA matrix. However, the shock wave travels much faster through the diamond ($c_L = 17.5 \text{ mm } \mu\text{s}^{-1}$) than the PMMA ($c_L = 2.6 \text{ mm } \mu\text{s}^{-1}$). An area (‘window’) of shocked diamond is visible in the interval immediately after the shock wave entered each diamond specimen (figure 2).

High time resolution was required because a window is imaged for less than $5 \mu\text{s}$. A shock wave travels through 5 mm of diamond in $\sim 300 \text{ ns}$, so an IFT of 100 ns with 50 ns exposure time was used. Interframe and exposure times were carefully

1
2
3
4
5
6
7
8 verified to within ± 2 ns using the UltranaC 501's electronic shutter monitor [14].
9
10 Each sequence consisted of 18 frames. Reliability of the technique was paramount,
11
12 so it was developed using embedded glass and sapphire particles [14].
13

14 Lighting is an important consideration for photography at high framing rates.
15 A reusable arc-discharge lamp was placed behind the specimen (back-lighting), in
16 the line of sight of the camera lens. The lamp discharged 2 kV across a 40 μ F
17 capacitor in ~ 10 μ s. The rise time was consistently 2–3 μ s and the total output
18 from a single flash was 80 J. Sheets of semi-transparent paper were placed between
19 the flash and the specimen to diffuse the light.
20
21
22
23
24

25 Impact was viewed through a clear glass portal in the side of the gas gun's
26 impact chamber. The distance between the lens and the specimen was ~ 1 m. The
27 lens aperture was opened as widely as possible in order to maximise light entering
28 the camera, as long as the depth of field did not become too small.
29
30
31

32 High-speed photographs were digitized and spatially calibrated using photographs
33 of the specimens that were taken prior to each experiment. Uncertainties in crack
34 velocity measurements reflect errors in spatial and temporal calibration. Velocity
35 measurements represent a lower bound on actual crack speed, because fracture sur-
36 faces can have a directional component perpendicular to the two-dimensional image
37 in the high-speed photographs. Additionally, a crack might only extend during part
38 of the 50 ns exposure time for each frame.
39
40
41
42
43
44
45
46

47 **3 Results**

48
49
50 [Insert table 2 about here]

51
52 [Insert figure 3 about here]

53 Figure 3 shows high-speed photographic frames from four embedded diamond ex-
54 periments (table 2). Labels on photographs indicate the time in microseconds after
55 the shock wave reached the embedded particle ('shock wave arrival'). The shock
56
57
58
59
60

1
2
3
4
5
6
7
8 wave travelling through the PMMA is imaged as a thick dark line moving from left
9 to right and extending vertically from the top to the bottom of each frame, ob-
10 scuring the embedded particle. The shock wave within the diamond traverses the
11 specimen approximately 3 times in 1 μs , by which time the shock in the PMMA
12 obscures roughly half the specimen. When the shock wave in the diamond first
13 reaches the back (right) edge of each specimen, $\sim 0.3 \mu\text{s}$ after shock wave arrival, a
14 'bow wave' is imaged moving into the surrounding matrix material. The specimens
15 are too thin for shock waves to be observed in the diamond itself.

16
17
18
19
20
21
22 [Insert table 3 about here]

23
24
25 Average crack velocities from experiment D5 are recorded in table 3. Labels for
26 these cracks are indicated in figure 3. The cracks extend in three dimensions and
27 do not necessarily propagate throughout the exposure time for each frame. The
28 tabulated measurements are averaged across the interframe time, and therefore
29 represent a lower bound on the maximum crack velocity. The values in table 3 are
30 typical of crack velocities measured in the embedded particle experiments. The
31 velocity of individual cracks can vary significantly as a function of time. Cracks
32 propagated at speeds ranging from less than $3 \text{ mm } \mu\text{s}^{-1}$ to greater than the Rayleigh
33 wave velocity (c_R). The latter are the subject of the discussion.

34
35
36
37
38
39
40
41 Table 4 records the average velocities of the fastest cracks ($v \gtrsim c_R$) measured
42 from high-speed photographs. Growth of these cracks is indicated by black arrows
43 in figure 3. All of the cracks initiated within $0.5 \mu\text{s}$ of shock wave arrival, except
44 cracks 2a and 3a, and all of the cracks propagate along $\{111\}$ cleavage planes.
45 Other, relatively fast cracks ($v \gtrsim 0.8c_R$) were observed in specimens D3 and D5.

46
47
48
49
50 [Insert table 4 about here]

51
52 [Insert figure 4 about here]

53
54
55
56
57
58
59
60 Figure 4 provides evidence that the growing dark lines observed in photographic
sequences should be identified as fracture surfaces. In figure 4(a), arrows denote

1
2
3
4
5
6
7
8 a crack propagating from the crystal centre of a semi-embedded diamond particle
9 in experiment D8. The crack moves along a $\{111\}$ plane at an average velocity of
10 $8.4 \pm 2.4 \text{ mm } \mu\text{s}^{-1}$, slower than the cracks recorded in table 4. A 31 mg fragment
11 recovered from experiment D8 (figure 4(b)) can be directly linked with the origi-
12 nal specimen due to the central, near-circular inclusion that is indicated by white
13 arrows in figures 4(a) and 4(b). In figure 4(b), the fracture surface denoted by the
14 arrow was formed by the crack in figure 4(a). Fracture surfaces of all recovered
15 diamond fragments have been analysed in detail [14], but provide little insight into
16 the mechanism of fast crack growth.
17
18
19
20
21
22
23
24

25 26 27 4 Discussion

28
29 Crack velocities in table 4 are between 2 and 37 % greater than c_R for the case when
30 $c_R = 10.3 \text{ mm } \mu\text{s}^{-1}$. Crack velocities greater than $0.9c_R$ have not been observed
31 for single mode I cracks in diamond or other materials [6]. Mode II cracks on a
32 weakened plane in a polymer [9] and cracks driven by pressurised fluid expansion
33 at the crack tip in sodium chloride [23] have been observed growing faster than
34 c_R . In the current research, high-speed cracks predominantly occurred when the
35 impact velocity was relatively high, so that large stresses were induced throughout
36 the diamond.
37
38
39
40
41
42
43

44 45 4.1 *Multiple Initiation Mechanism*

46
47 The most likely explanation for the elevated crack speeds observed in the current
48 experiments is a ‘multiple initiation’ mechanism (figure 5). This mechanism ac-
49 counts for the presence of flaws near a crack tip in a real material. If the time
50 $(t_3 - t_1)$ and length (Δx) scales defined in figure 5 are smaller than the experi-
51 mental resolution, the fracture surface will appear to grow as a single, fast-moving
52 crack. Experiments carried out by Ravi-Chandar and Knauss [26] concluded that
53
54
55
56
57
58
59
60

1
2
3
4
5
6
7
8 brittle fracture could occur by way of a similar mechanism, involving coalescence
9 of microcracks.

10
11 [Insert figure 5 about here]

12
13 The value of Δx can be constrained using high-speed photographs. In the case
14 of crack 3a (figure 3(c)), the fracture appears to grow from the developing central
15 region (as indicated by the black arrows) as well as from a feature near the edge
16 of the disc, denoted by a white arrow in the frame 0.7 μs after shock wave arrival.
17 The features at either end of the eventual fracture are ~ 2 mm apart and join up
18 in the 100 ns separating the frames 0.7 and 0.8 μs after shock wave arrival. The
19 other fast cracks appear to propagate in a single direction; cracks 1a (figure 3(a))
20 and 5h (figure 3(d)) do so over three frames. The upper limit of $t_3 - t_1$ is the
21 interframe time, 100 ns. The limiting velocity for single cracks restricts Δx to less
22 than 2 mm. Microscopic flaws incorporated during octahedral growth commonly
23 populate $\{111\}$ planes in diamond, and flaws large enough to produce clearly visible
24 birefringence fringes occur with a frequency of approximately 10 mm^{-2} on natural
25 diamond surfaces [24]. It is likely that multiple initiation occurs on microscopic
26 scales. The proposed mechanism does not require that secondary flaws lie near
27 specimen surfaces, where flaws in crystal specimens are most prevalent. Secondary
28 fractures in crack 1a and the cracks in specimen D5 would initiate a significant
29 distance from specimen edges.
30
31
32
33
34
35
36
37
38
39
40
41
42
43
44

45 In isotropic materials, it is energetically favourable for fast cracks to 'branch'
46 into the plane on which tensile stress is maximized, which lies at a finite angle
47 to the original crack plane [5]. When conditions are almost conducive to crack
48 branching, microcracks can initiate ahead of the crack tip without extending into
49 a full crack branch, forming a roughened texture on the fracture surface [6]. Full
50 crack branches are therefore generated by secondary fractures ahead of the crack tip.
51 This mechanism is identical to the multiple initiation mechanism except that, in
52
53
54
55
56
57
58
59
60

1
2
3
4
5
6
7
8 diamond, preference for $\{111\}$ cleavage suppresses branching fractures and restricts
9 secondary fractures to the $\{111\}$ cleavage planes.
10

11 On a single weak cleavage plane containing particularly large flaws, abundant
12 flaws and / or significant internal stresses, multiple fractures could be nucleated
13 independently. Alternatively, if the stress field near the tip of a secondary flaw is
14 intensified by the propagating primary crack, multiple fractures could be linked.
15 Stress intensification would be caused by the stress field surrounding the tip of the
16 primary crack, or stress waves radiating from the propagating primary crack tip.
17
18 Linked initiation is more likely when Δx is small.
19
20
21
22
23
24

25 Secondary initiation preferentially occurs on the same cleavage plane as the pri-
26 mary fracture. If this was not the case, multiple fractures would be observed on
27 $\{111\}$ planes adjacent to secondary fractures, or conchoidal fracture would be re-
28 quired to join primary and secondary fractures on separate cleavage planes. Neither
29 phenomenon is observed in the high-speed photographs. This observation requires
30 that, if secondary initiation is independent, the cleavage plane of a fast crack must
31 be particularly weak in comparison with nearby cleavage planes. If secondary ini-
32 tiation is linked, the energetic expense of conchoidal fracture requires that secondary
33 cracks lie on the same cleavage plane as the primary crack.
34
35
36
37
38
39
40
41

42 Further experimental observations of cracks in isotropic materials are consistent
43 with the multiple initiation mechanism. Crack branching in isotropic materials
44 is dependent on flaws lying within the stress field surrounding the crack tip [6],
45 as is the case with diamond. Increased loading results in more frequent crack
46 branching in isotropic materials [6]; when branching is suppressed, increased loading
47 produces higher crack velocities (as observed in the current study) due to more
48 frequent secondary fracture. A very similar phenomenon to the multiple initiation
49 mechanism is observed in high-speed photography of glass rod impact experiments
50 [25], when secondary fractures are sometimes observed further from the impact
51
52
53
54
55
56
57
58
59
60

1
2
3
4
5
6
7
8 plane than the failure front.

9
10 The multiple initiation mechanism is similar to the Burridge-Andrews mecha-
11 nism for intersonic mode II shear cracks [7]. Burridge [27] found a peak in the ana-
12 lytical shear stress field propagating slightly ahead of a mode II crack tip at speeds
13 close to c_R . Working independently with a numerical finite-difference scheme, An-
14 drews [28] found that a secondary slip region nucleates ahead of the crack under
15 similar conditions. New fractures coalesce with the original crack and the fracture
16 surface can extend intersonically.

17
18 In both the Burridge-Andrews and multiple initiation mechanisms, fracture is
19 confined to a single plane by material anisotropy and secondary fractures nucleate
20 ahead of a propagating crack tip. However, multiple initiation requires stress in-
21 tensification at flaws ahead of the crack tip whereas the stress field near the tip
22 of a mode II crack has an intrinsic local maximum. Neither mechanism strictly
23 describes propagation of a single (primary) crack, but both explain experimental
24 observations of fracture surfaces that extend at a rate that is faster than c_R .

25
26 The two mechanisms blur the distinction between single and multiple cracks.
27 Classification of real single cracks depends on the characteristic length scales of
28 non-idealities (e.g. flaws) in real materials. These length scales (relative to crack
29 velocity) are typically too small for multiple cracks to be resolved in experiments.

4.2 *Other Possible Explanations*

30
31 It is unlikely that the fast cracks in the current research extend by way of a pre-
32 dominantly mode II (shearing) mechanism. They constitute a significant fraction
33 of all the macroscopic cracks observed in experiments D1, D2, D3 and D5; cracks
34 preferentially nucleate in pure tension. The cracks propagate in multiple directions
35 in individual specimens, rather than a particular direction favoured by macroscopic
36 shear stress. There is no evidence of conchoidal fracture accompanying the fast

1
2
3
4
5
6
7
8 cracks, unlike the fast mode II fractures observed by Rosakis [7].
9

10 Cracks are only imaged once they have opened a distance equal to half the
11 wavelength of the illuminating light. A crack could erroneously appear to travel at
12 an elevated velocity if the opening angle near the crack tip varied significantly over
13 time scales comparable to the IFT. Considering the specimen brittleness, image
14 resolution and short IFT in the current experiments, such variation is unlikely to
15 be significant.
16
17

18 The propagating fractures could be single mode I cracks moving faster than the
19 theoretical limiting speed under linear elastodynamics ($\sim c_R$ [5, 7]). The effects
20 of the zone of plastically deformed material present at any real crack tip are not
21 well understood. However, diamond is highly brittle, so any disparity between the
22 theory for single cracks and the current observations is more likely to be caused by
23 experimental conditions than any theoretical shortcomings.
24
25
26
27
28
29
30
31
32

33 5 Conclusions

34 Well-calibrated high-speed photographs have been used to observe six fracture sur-
35 faces extending at velocities between c_R and $1.3c_R$ in shocked diamond. These
36 velocities are higher than the limiting velocities previously proposed in theoretical
37 and practical studies of single mode I cracks in diamond and other material.
38
39
40
41
42
43

44 The most likely explanation for the fast crack measurements has been explained
45 using a multiple initiation mechanism. In this mechanism, single cracks coalesce
46 with secondary cracks on the same cleavage plane in an anisotropic material. The
47 coalescence is not observed in experiments due to resolution limits and the fracture
48 surface appears to extend faster than the speed of a single crack. Multiple initiation
49 is identical to the mechanism that causes crack branching in an isotropic material,
50 except that secondary fractures ahead of the crack tip are restricted to the same
51 cleavage plane as the initial crack. This mechanism is also consistent with high-
52
53
54
55
56
57
58
59
60

1
2
3
4
5
6
7
8 speed photography of shocked glass and previous experimental studies of single
9 crack propagation.

10
11 The multiple initiation mechanism has many similar features to the Burridge-
12 Andrews mechanism, which is widely used to describe fast mode II crack propaga-
13 tion. It is apparent that analyses of single cracks are restricted by the effects of
14 flaws in real materials and the limits of resolution in experimental diagnostics.
15
16
17
18
19
20

21 **6 Acknowledgements**

22
23 The authors thank Dr. Alan Guest and De Beers Consolidated Mines Ltd. for
24 support of this research. Specimens were prepared by Ray Flaxman and Daniel
25 Cross. High-speed photography at the Cavendish Laboratory is funded by the
26 Engineering and Physical Sciences Research Council.
27
28
29
30
31
32

33 **References**

- 34
35
36 [1] A. A. Griffith, *Phil. Trans. R. Soc. Lond. A*, **221** 163 (1920).
37
38 [2] B. R. Lawn, *Fracture of Brittle Solids*, 2nd edition (Cambridge University
39 Press, Cambridge, 1993).
40
41
42 [3] N. F. Mott, *Engineering* **165** 16 (1948).
43
44 [4] K. B. Broberg, *Cracks and Fracture* (Academic Press, London, 1999).
45
46 [5] L. B. Freund, *Dynamic Fracture Mechanics* (Cambridge University Press,
47 Cambridge, 1990).
48
49 [6] J. E. Field, *Contemp. Phys.* **12** 1 (1971).
50
51 [7] A. J. Rosakis, *Advances in Physics* **51** 1189 (2002).
52
53
54
55
56
57
58
59
60

- 1
2
3
4
5
6
7
8 [8] M. Bouchon, M. P. Bouin, H. Karabulut, N. Toksoz, M. Dietrich and A. J.
9 Rosakis, *Geophys. Res. Letts.* **28** 2723 (2001).
10
11
12 [9] A. J. Rosakis, O. Samudrala and D. Coker, *Science* **284** 1337 (1999).
13
14
15 [10] L. B. Freund, *J. Geophys. Res.* **84** 2199 (1979).
16
17
18 [11] J. E. Field and C. J. Freeman, *Phil. Mag. A* **43** 595 (1981).
19
20 [12] J. E. Field, Chapter 12 in *The Properties of Natural and Synthetic Diamond*,
21 edited by J. E. Field (Academic Press, London, 1992).
22
23
24 [13] S. Ramaseshan, *Proc. Indian Acad. Sci.* **A24** 114 (1946).
25
26
27 [14] G. R. Willmott, *Shock studies of kimberlite, diamond and brittle embedded*
28 *particles*. PhD thesis, University of Cambridge (2004).
29
30
31 [15] R. H. Telling, C. J. Pickard, M. C. Payne and J. E. Field, *Phys. Rev. Lett.* **84**
32 5160 (2000).
33
34
35 [16] I. A. Viktorov, *Rayleigh and Lamb Waves: Physical Theory and Applications*
36 (Plenum Press, New York, 1967).
37
38
39 [17] F. F. Voronov and L. F. Vereshchagin, *Phys. Metals Metallog.* **11** 111 (1961).
40
41
42 [18] T. S. Duffy and T. J. Ahrens, *J. Geophys. Res.* **97** 4503 (1992).
43
44
45 [19] J. E. Field, *Proc. R. Institution* **60** 195 (1988).
46
47
48 [20] S. F. Ray, *High Speed Photography and Photonics* (Focal Press, London, 1997).
49
50
51 [21] F. P. Bowden and J. E. Field, *Proc. R. Soc. Lond. A* **282** 331 (1964).
52
53
54 [22] N. K. Bourne, Z. Rosenberg, D. J. Johnson, J. E. Field, A. E. Timbs and R.
55 P. Flaxman, *Meas. Sci. Technol.* **6** 1462 (1995).
56
57
58 [23] S. Winkler, D. R. Curran and D. A. Shockey, *Int. J. Fracture* **6** 271 (1970).
59
60

- 1
2
3
4
5
6
7
8 [24] A. R. Lang, Nature **213** 248 (1967).
9
10 [25] G. R. Willmott and D. D. Radford, J. Appl. Phys. **97** 093522 (2005).
11
12 [26] K. Ravi-Chandar and W. G. Knauss, Int. J. Fract. **25** 247 (1984).
13
14 [27] R. Burridge, Geophys. J. Royal Astronom. **35** 439 (1973).
15
16 [28] D. J. Andrews, J. Geophys. Res. **81** 5679 (1976).
17
18
19
20
21
22
23
24
25
26
27
28
29
30
31
32
33
34
35
36
37
38
39
40
41
42
43
44
45
46
47
48
49
50
51
52
53
54
55
56
57
58
59
60

Table 1: Physical characteristics of diamond [12]. The values for Young's modulus (E) and Poisson's ratio (ν) correspond, respectively, to E_{111} and the 'isotropic aggregate value' of ν [12]. Wave velocity values correspond to a state of uniaxial strain in which the tabulated values of E and ν are used in calculations. Variation of these values is discussed in the text.

Density	ρ_0	3.52 g cm ⁻³
Young's Modulus	E	1050 GPa
Poisson's Ratio	ν	0.07
Longitudinal Elastic Wave Velocity	c_L	17.5 mm μ s ⁻¹
Transverse Elastic Wave Velocity	c_S	11.6 mm μ s ⁻¹
Rayleigh Wave Velocity	c_R	10.3 mm μ s ⁻¹
Practical Tensile Strength	σ_f	3.75 GPa
Theoretical Fracture Surface Energy	γ_{111}	5.3 J m ⁻²
Critical Stress Intensity Factor	K_{IC}	3.4 MN m ^{-3/2}
Refractive Index	n	2.417

Table 2: Summary of the conditions for the five impact experiments cited in this paper.

Experiment	Impact Velocity	Specimen Details		
	(mm μs^{-1})	Plane of Slice	Quality	Mass (± 1 mg)
D1	506 ± 3	{110}	Cracked	126
D2	503 ± 3	{110}	Clean	168
D3	296 ± 1	{100}	Cracked	208
D5	407 ± 2	{111}	Clean	156
D8	453 ± 2	{111}	Cracked	148

Table 3: Crack propagation velocities for the eight cracks from experiment D5, as labelled in figure 3(e).

Crack	Average Crack Velocity ($\text{mm } \mu\text{s}^{-1}$) in Time Interval				
	0.2–0.3 μs	0.3–0.4 μs	0.4–0.5 μs	0.5–0.6 μs	0.6–0.7 μs
5a	2.9 ± 0.6	5.9 ± 1.0	0.5 ± 1.0	11.4 ± 0.7	6.0 ± 0.9
5b	-	2.7 ± 0.7	3.7 ± 0.7	10.8 ± 0.7	1.1 ± 0.8
5c	-	-	3.1 ± 0.5	-	-
5d	-	2.6 ± 0.5	8.8 ± 0.7	3.1 ± 0.8	-
5e	-	-	-	2.6 ± 0.5	-
5f	-	1.5 ± 0.7	5.1 ± 0.8	-	-
5g	-	-	7.1 ± 0.7	6.6 ± 0.8	-
5h	2.7 ± 0.5	3.9 ± 0.8	3.5 ± 0.9	12.6 ± 1.0	9.0 ± 1.2

Table 4: Summary of crack velocity measurements near or above c_R in diamond. ‘Successive measurements’ refers to the number of interframe velocities measured over adjacent 100 ns intervals in high-speed sequences.

Crack	Successive Measurements	Average Velocity ($\text{mm } \mu\text{s}^{-1}$)	Shown in Figure
1a	2	10.5 ± 0.9	3(a)
2a	1	12.2 ± 1.4	3(b)
3a	1	14.1 ± 1.1	3(c)
5a	1	11.4 ± 0.7	3(d)
5b	1	10.8 ± 0.7	3(d)
5h	2	10.8 ± 0.8	3(d)

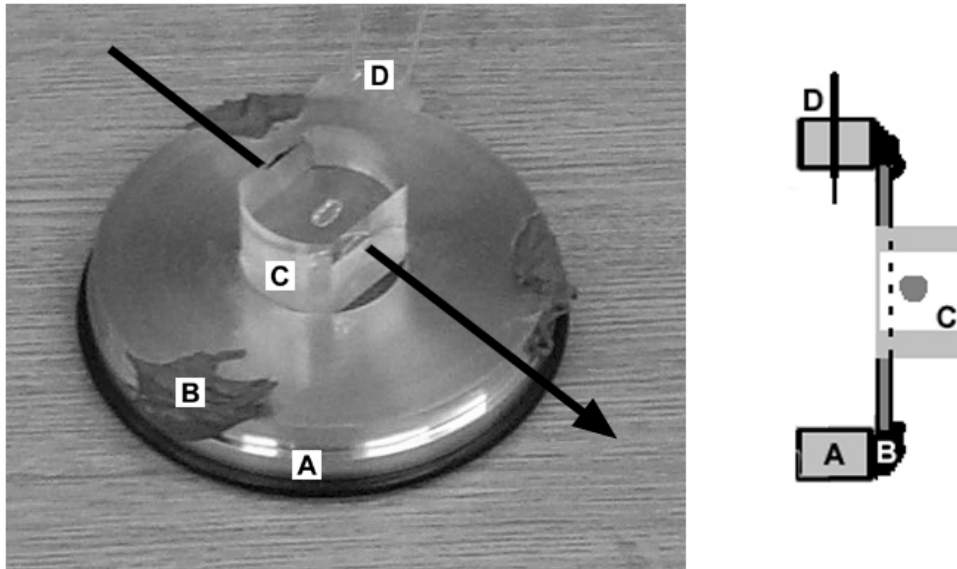


Figure 1: An embedded diamond specimen is photographed (left) with an arrow indicating the line of view for the high-speed camera. A schematic cross-section of the specimen (right) is shown from the viewpoint of the camera; the flyer plate arrives from the left in this diagram. Labelled features are:

- (A) Aluminium alignment ring, thickness 15 mm, inner diameter 55 mm.
- (B) Chemical metal epoxy, holding a 2 mm thick aluminium plate in place.
- (C) Cylindrical polymer block, flush with the impact face, diameter 30 mm and thickness ~ 15 mm. Two flat polished faces for photography are ~ 20 mm apart. Embedded diamonds were emplaced ~ 3 mm from the impact face.
- (D) 'Make' trigger; two wires protrude through holes drilled into the alignment ring ~ 3 mm from the impact face. The actual positions of the embedded diamond and the make trigger were measured to within ± 0.1 mm.

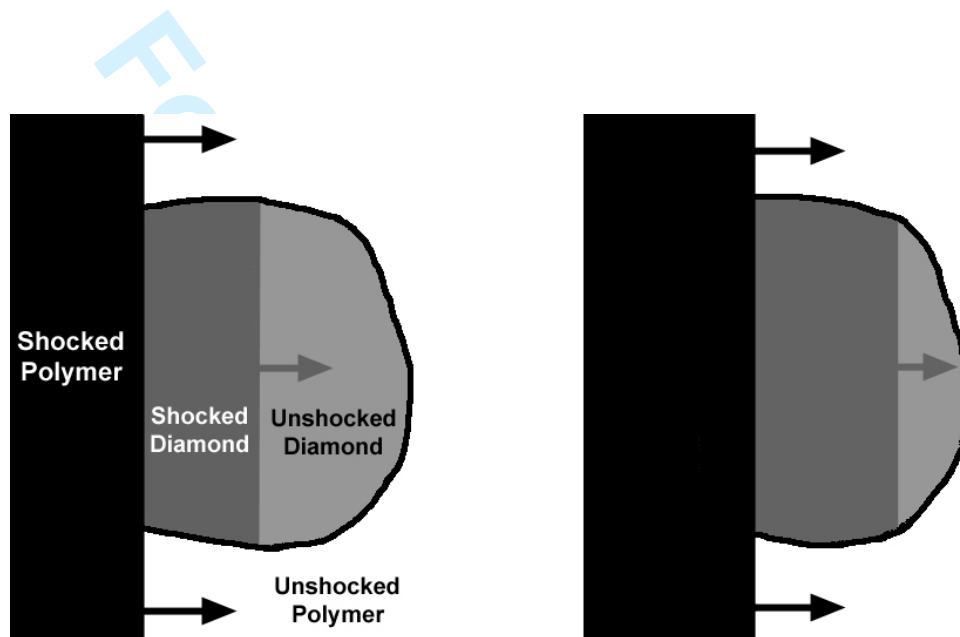


Figure 2: Two successive, schematic frames from a high-speed sequence showing the relative positions of shock waves and their effect on the imaging of an embedded diamond specimen. The 'window' is that part of the diamond that is unobscured by the shock in the polymer. In some experiments, the dark band in the polymer is thin enough for the diamond to be observed after the leading edge of the shock wave has passed.

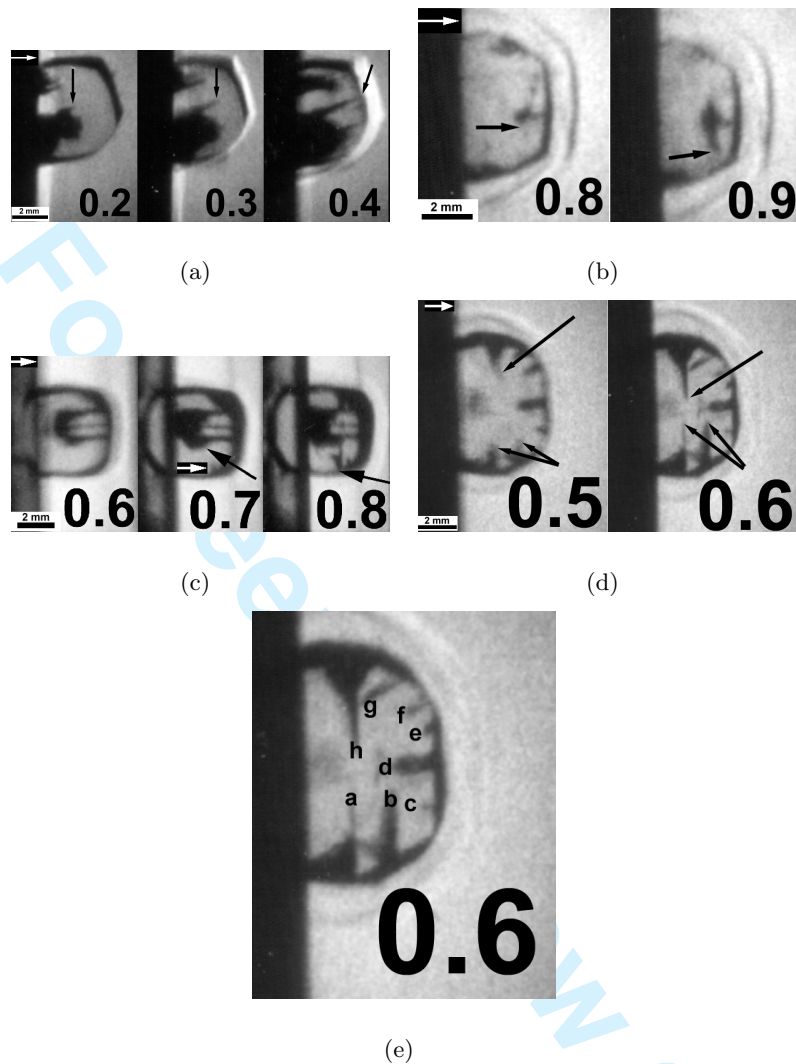


Figure 3: Frames from four high-speed sequences, with propagating fast cracks (table 4) denoted by arrows. The white arrow in the first frame of each sequence points to the edge of the dark, vertical shock front in the PMMA matrix. Each frame is labelled with the time in microseconds after shock wave arrival. Figures 3(a), 3(b), 3(c) and 3(d) show frames from experiments D1, D2, D3 and D5 respectively; experimental details are recorded in table 2. **The white arrow in the second frame of figure 3(c) is discussed in the text.** Figure 3(e) shows the labels for eight cracks in experiment D5, with velocities recorded in table 3.

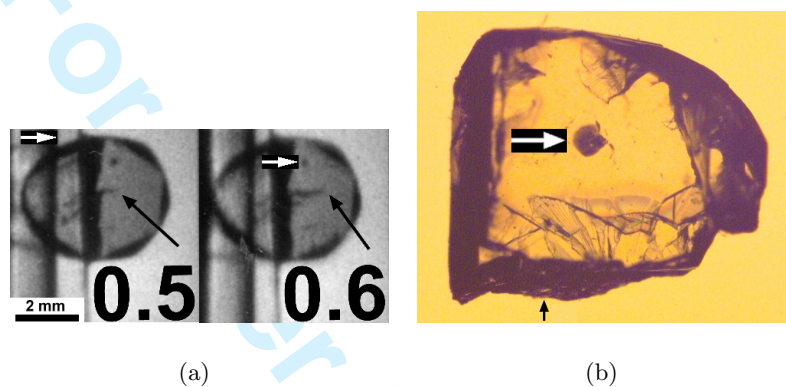


Figure 4: Figure 4(a) shows frames from the high-speed sequence for experiment D8, with each frame labelled with the time in microseconds after shock wave arrival. A white arrow in the first frame points to the edge of the dark, vertical shock front in the PMMA matrix. The specimen was only partially embedded in PMMA: the second vertical line, to the right of the shock front, is the edge of the PMMA matrix. Experimental details are recorded in table 2. Figure 4(b) shows a diamond fragment recovered from experiment D8. A near-circular inclusion in the specimen is indicated by white arrows in figure 4(b) and the second frame of figure 4(a). The propagating crack that is denoted by arrows in Figure 4(a) creates the fracture surface next to the arrow in Figure 4(b).

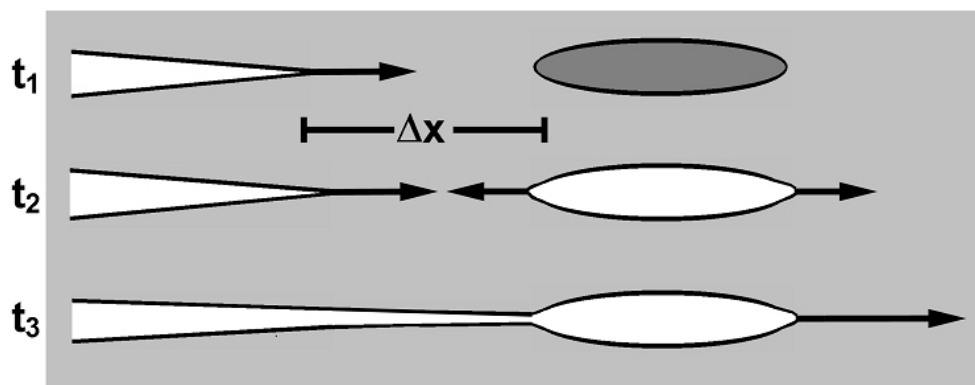


Figure 5: Schematic description of the multiple initiation mechanism for extension of fracture surfaces. Arrows indicate propagating crack tips. Initially (t_1), a primary crack propagates towards a static flaw on the same $\{111\}$ cleavage plane at velocity v . When the separation of the flaw and the primary crack tip is Δx , the flaw extends into secondary cracks that move in both directions along the cleavage plane (t_2). The primary and secondary cracks eventually coalesce into one fracture (t_3). If the intermediate step is not observed, the crack appears to travel faster than v .